Earth and Planetary Science Letters 387 (2014) 240–251

Contents lists available at ScienceDirect

Earth and Planetary Science Letters

www.elsevier.com/locate/epsl

Deglacial $\delta^{18}O$ and hydrologic variability in the tropical Pacific and Indian Oceans ☆

Fern T. Gibbons [a,*], Delia W. Oppo [b], Mahyar Mohtadi [c], Yair Rosenthal [d,e], Jun Cheng [f], Zhengyu Liu [g,h], Braddock K. Linsley [i]

[a] MIT/WHOI Joint Program in Oceanography, Woods Hole Oceanographic Institution, Woods Hole, MA 02543, USA
[b] Department of Geology and Geophysics, Woods Hole Oceanographic Institution, Woods Hole, MA 02543, USA
[c] MARUM-Zentrum für Marine Umweltwissenschaften, University of Bremen, Bremen, Germany
[d] Institute of Marine and Coastal Sciences, Rutgers, The State University, New Brunswick, NJ, 08901, USA
[e] Department of Geology, Rutgers, The State University, New Brunswick, NJ 08901, USA
[f] School of Marine Sciences, Nanjing University of Information Sciences and Technology, Nanjing 210044, PR China
[g] Center for Climate Research and Dept. Atmospheric and Oceanic Sciences, University of Wisconsin–Madison, Madison, WI 53706, USA
[h] Lab. of Ocean-Atmos. Studies, School of Physics, Peking University, Beijing 100871, PR China
[i] Lamont-Doherty Earth Observatory of Columbia University, Palisades, NY 10694, USA

ARTICLE INFO

Article history:
Received 5 August 2013
Received in revised form 14 November 2013
Accepted 14 November 2013
Editor: J. Lynch-Stieglitz

Keywords:
Indo-Pacific
Eastern Equatorial Pacific
$\delta^{18}O$ of seawater
deglaciation
heat transport

ABSTRACT

Evidence from geologic archives suggests that there were large changes in the tropical hydrologic cycle associated with the two prominent northern hemisphere deglacial cooling events, Heinrich Stadial 1 (HS1; ~19 to 15 kyr BP; kyr BP = 1000 yr before present) and the Younger Dryas (~12.9 to 11.7 kyr BP). These hydrologic shifts have been alternatively attributed to high and low latitude origin. Here, we present a new record of hydrologic variability based on planktic foraminifera-derived $\delta^{18}O$ of seawater ($\delta^{18}O_{sw}$) estimates from a sediment core from the tropical Eastern Indian Ocean, and using 12 additional $\delta^{18}O_{sw}$ records, construct a single record of the dominant mode of tropical Eastern Equatorial Pacific and Indo-Pacific Warm Pool (IPWP) hydrologic variability. We show that deglacial hydrologic shifts parallel variations in the reconstructed interhemispheric temperature gradient, suggesting a strong response to variations in the Atlantic Meridional Overturning Circulation and the attendant heat redistribution. A transient model simulation of the last deglaciation suggests that hydrologic changes, including a southward shift in the Intertropical Convergence Zone (ITCZ) which likely occurred during these northern hemisphere cold events, coupled with oceanic advection and mixing, resulted in increased salinity in the Indonesian region of the IPWP and the eastern tropical Pacific, which is recorded by the $\delta^{18}O_{sw}$ proxy. Based on our observations and modeling results we suggest the interhemispheric temperature gradient directly controls the tropical hydrologic cycle on these time scales, which in turn mediates poleward atmospheric heat transport.

1. Introduction

In the North Atlantic, the warming of the last deglaciation was punctuated by two millennial-scale coolings. HS1 is characterized by very cold sea surface temperatures (SSTs). Heinrich Event 1 (H1; 17.5 to 16 kyr BP) occurred during the final portion of HS1 and was first identified by large abundance peaks of ice rafted debris in sediment cores (Heinrich, 1988; Hemming, 2004). The Younger Dryas also coincides with ice rafted debris in North Atlantic sediments and cooler temperatures (Bond et al., 1993). The cause of these coolings in the North Atlantic is still debated, but the leading hypothesis is that they resulted from freshwater input at the sites of deep-water formation, which altered the Meridional Overturning Circulation (Broecker, 1991), consistent with geologic evidence (Hall et al., 2006; McManus et al., 2004; Stanford et al., 2011). The source of freshwater was likely iceberg discharge for H1 (Bond et al., 1992) and Heinrich Stadial 1 (Stanford et al., 2011). Evidence of the fresh water source is more elusive for the Younger Dryas (Broecker, 2006), though recent work suggests freshwater may have been routed through the Arctic (e.g. Murton et al., 2010).

* Corresponding author at: The Nature Conservancy, 4245 North Fairfax Drive, Suite 100, Arlington, VA, 22203, USA.
E-mail address: ferngibbons@gmail.com (F.T. Gibbons).

0012-821X/$ – see front matter
http://dx.doi.org/10.1016/j.epsl.2013.11.032

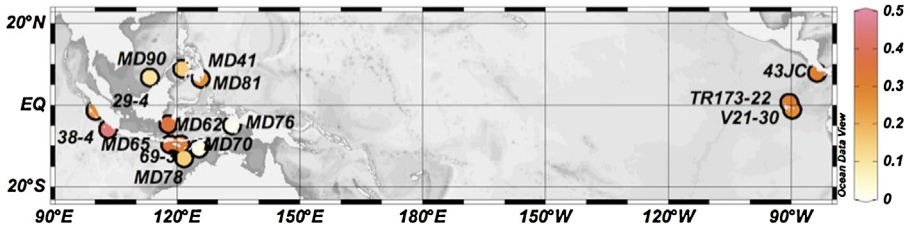

Fig. 1. Core locations and loading for the first principal component (PC1) of $\delta^{18}O_{sw\text{-}iv}$ records. Cores with higher values contribute more to the first principal component (shown in Fig. 5). Values for cores from the Indo-Pacific and Eastern Equatorial Pacific are approximately equal (see also color online version).

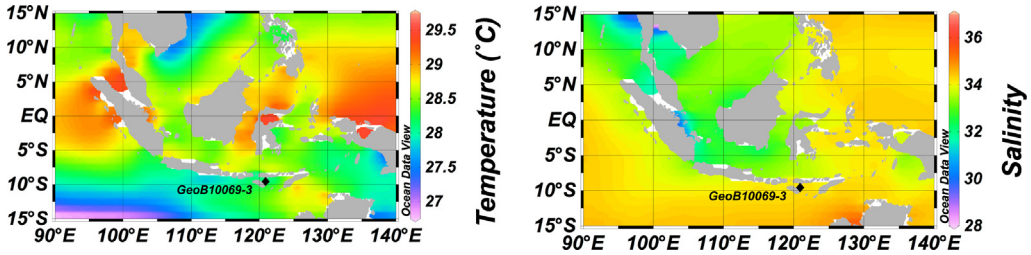

Fig. 2. Location of core GeoB10069-3 on maps of mean annual modern SST (Locarnini et al., 2006) (left) and sea surface salinity (Antonov et al., 2006) (right).

Table 1

Core ID, location	Reference	Lat./Long.	Water depth (m)	Average sample interval (yr)	Loadings for PC1
GeoB10029-4, Eastern Indian Ocean,	Mohtadi et al., 2010	1°30′S, 100°8′E	962	600	0.27
GeoB10038-4, Eastern Indian Ocean	Mohtadi et al., 2010	5°56′S, 103°15′E	1,819	560	0.45
GeoB10069-3, Savu Sea	This text	9°36′S, 120°55′E	1,250	190	0.3
MD97-2141, Sulu Sea	Rosenthal et al., 2003	8°47′N, 121°17′E	3,633	90	0.15
MD98-2162, S. Makassar St.	Visser et al., 2003	4°41′S, 117°54′E	1,855	415	0.36
MD98-2165, Sumba St.	Levi et al., 2007	9°39′S, 118°20′E	2,100	200	0.35
MD98-2170, Timor Sea	Stott et al., 2002/Stott et al., 2007	10°36′S, 125°23′E	832	300	0.02
MD98-2176, Seram Sea	Stott et al., 2002/Stott et al., 2007	5°00′S, 133°27′E	2,382	75	0.01
MD98-2181, W. Pacific, Mindanao	Stott et al., 2002/Stott et al., 2007	6°27′N, 125°50′E	2,114	50	0.26
MD01-2378, Timor Sea	Xu et al., 2008/Sarnthein et al., 2011	13°05′S, 121°47′E	1,783	125	0.15
MD01-2390, South China Sea	Steinke et al., 2008	6°38′N, 113°25′E	1,545	200	0.11
ME0005A-43JC, Eastern Eq. Pacific	Benway et al., 2006	7°51′N, 83°37′W	1,368	240	0.3
TR163-22, Eastern Eq. Pacific	Lea et al., 2006	0°31′N, 92°24′W	2,830	270	0.31
V21-30, Eastern Eq. Pacific	Koutavas et al., 2002	1°13′S, 89°41′E	617	430	0.27

In contrast to the large temperature signal in the extratropics, these millennial-scale fluctuations only show a small or even no signal in tropical SST records (Kiefer and Kienast, 2005; Stott et al., 2007). However tropical terrestrial records indicate large and pervasive changes in tropical hydrology associated with both HS1 and the Younger Dryas (e.g. Stager et al., 2011; Tierney et al., 2008; Wang et al., 2007; Yuan et al., 2004). The spatial patterns of hydrologic changes over land are consistent with southward shifts of the coupled monsoon-Intertropical Convergence Zone (ITCZ) systems during North Atlantic cold events (see for example, Stager et al. (2011) and Oppo and Curry (2012) for recent compilations of H1 terrestrial responses), although there is also evidence of generally weaker African and Asian monsoons (Stager et al., 2011; Tierney et al., 2008).

By contrast, and as we discuss in more detail below, marine records from the Indo-Pacific Warm Pool (IPWP) provide conflicting information on deglacial hydrologic variability, with some records suggesting higher salinity during North Atlantic cold events, others suggesting greater river runoff, and still others suggesting no change. In a few cases, marine records appear to conflict with nearby terrestrial records. There are even instances of disagreement among geographically close marine records that use the same proxy. In the Eastern Indian Ocean (MD98-2165, Table 1) $\delta^{18}O_{sw}$ is higher during both HS1 and the Younger Dryas (Levi et al., 2007), suggesting a reduction in the intensity of the hydrologic cycle. By contrast, $\delta^{18}O_{sw}$ reconstructions from the nearby Timor Sea (MD98-2170 and MD01-2378; for location see Supplementary Fig. 1) suggest no changes during these events (Stott et al., 2007; Xu et al., 2008).

Furthermore, some studies suggest that changes in the mean Pacific state, notably the east–west SST gradient changes, were a dominant control on tropical Pacific hydrology during these events (Levi et al., 2007; Rosenthal et al., 2003; Stott et al., 2002), while others have suggested that the data are consistent with a meridional migration of the ITCZ (Leduc et al., 2009).

Here, we examine the influence of the abrupt North Atlantic events on tropical hydrology from a marine perspective using a more comprehensive dataset and a transient climate model simulation. We present a new high-resolution record of $\delta^{18}O_{sw}$ of the mixed layer planktic foraminifera *Globigerinoides ruber* (*G. ruber*) from the Savu Sea, which is supplied by Indonesian Throughflow water entering the Indian Ocean through the Ombai Strait (Figs. 1 and 2, Supplementary Fig. 1). Using Mg/Ca-based temperature reconstructions, the $\delta^{18}O$ of calcite, and following previous work (e.g. Lea et al., 2000), we calculated the $\delta^{18}O_{sw}$ at this site over the past 35 kyr. We combine our new record with published $\delta^{18}O_{sw}$ reconstructions from reasonably well-dated and high-resolution records from throughout the IPWP and the Eastern Equatorial Pacific Ocean (Fig. 1, Table 1) to determine the dominant temporal and spatial patterns of deglacial $\delta^{18}O_{sw}$ change. Furthermore, we analyze a transient simulation in a state-of-art Coupled General

Circulation Model (CGCM) to shed light on the mechanisms of deglacial $\delta^{18}O_{sw}$ and tropical hydrological variability.

Previous studies have investigated Holocene changes in regional ocean circulation due to the opening of the passage between the South China Sea and the Indonesian Seas at ~10 kyr BP. Rising sea level flooded the Sunda Shelf and influenced $\delta^{18}O_{sw}$ and freshwater gradients in the region (Ding et al., 2002; Linsley et al., 2010; Rosenthal et al., 2003; Xu et al., 2010). We use many of the same records, however, our focus is on coherent larger scale, basin-wide variations in tropical rainfall during millennial-scale events.

2. Materials and methods

Sediment core GeoB10069-3 (9°36′S, 120°55′E, 1250 m, Fig. 2) was retrieved from the Savu Basin in the Eastern Indian Ocean. The Savu Basin is in the path of one of the outflow passages of the Indonesian Throughflow. Today, minimum temperatures at GeoB10069-3 are ~26 °C and occur in the boreal summer (all seasons are with respect to the Northern Hemisphere) and maximum temperatures are ~31 °C.

Stable isotope measurements from GeoB10069-3 were made at Bremen University on a Finnigan MAT251. Long-term precision of $\delta^{18}O_{calcite}$ measurements is 0.07‰, based on repeated measurements of a suite of standards. Approximately 5–20 individual tests were used for each measurement.

For GeoB10069-3, approximately 40 *G. ruber* tests (212–300 μm) were used for each Mg/Ca measurement. Samples were cleaned with a full trace metal cleaning procedure, including oxidative and reductive steps (Boyle and Keigwin, 1985/1986; Rosenthal et al., 1997). Samples were run on either an Element2 ICP-MS at Woods Hole Oceanographic Institution or an Element XR ICP-MS at Rutgers University. Internal reproducibility based on repeated measurements of consistency standards is ~1%. Replicates were run for 17 samples (not homogenized prior to cleaning). The variance ($\sigma^2_{Mg/Ca}$) was 0.21 mmol/mol.

We also compiled published $\delta^{18}O_{calcite}$ (Supplementary Fig. 2) and Mg/Ca (Supplementary Fig. 3) data from planktic foraminifera from reasonably well-dated, high-resolution records from throughout the Eastern Indian and Pacific tropics (Fig. 1, Table 1). All records are based on data from *G. ruber*, with the exception of V21-30, which utilized *Globigerinoides sacculifer* (*G. sacculifer*). In our compilation, we examine the past 20 kyr, determined by the maximum length of several published records.

To the extent possible, we have treated the Mg/Ca data from all the cores in the same manner in order to better allow us to compare datasets. Where possible, Mg/Ca was converted to temperature based on cleaning technique, though in some cases, the calibration from the original publication was used (see supplementary discussion). Regional core-top data suggest that an equation that corrects for dissolution is not necessary at this site (Gibbons, 2012).

Following Lea et al. (2000), the Mg/Ca-based temperature and $\delta^{18}O_{calcite}$ were used to calculate $\delta^{18}O_{sw}$ estimates. $\delta^{18}O_{sw}$ are corrected for mean ocean $\delta^{18}O_{sw}$ changes due to global ice volume change ($\delta^{18}O_{sw\text{-}iv}$; see methods and supplementary discussion), assuming that these were instantaneously registered in the surface tropical Indo-Pacific. This corrected $\delta^{18}O_{sw\text{-}iv}$ likely reflects mainly the local sea surface salinity (SSS) changes.

We propagate the uncertainty introduced by the Mg/Ca measurement, the Mg/Ca-temperature equation, the $\delta^{18}O_{calcite}$ measurement, the $\delta^{18}O$-paleotemperature equation, and the global correction for ice volume (see supplementary discussion for details). For a single measurement the standard deviation (1σ) is approximately ±0.3‰; thus changes are not inferred from a single data point.

The age model for GeoB10069-3 is based on 17 radiocarbon dates from planktic foraminifera. All age models are based on radiocarbon dates on planktic foraminifera (for data, more details on material and methods, and confidence intervals on age control points see supplementary material). We use Principal Component Analysis (Jolliffe, 2002) to determine the dominant mode of $\delta^{18}O_{sw\text{-}iv}$ variability. These analyses were performed after the data from each record was averaged in 500-yr bins.

We use output from a transient simulation of the last 22 kyr from the National Center for Atmospheric Research's Community Climate System Model version 3 (CCSM3) (Liu et al., 2009) to explore the mechanisms giving rise to the spatial $\delta^{18}O_{sw\text{-}iv}$ patterns we observe, the reasons for apparent discrepancies between $\delta^{18}O_{sw\text{-}iv}$ and terrestrial precipitation records in our southern Indo-Pacific Warm Pool study area, and the implications of a strong correlation between the dominant $\delta^{18}O_{sw\text{-}iv}$ mode and the interhemispheric temperature gradient, discussed in Section 4.4. The model was initiated with glacial boundary conditions, and deglacial variability was forced by realistic insolation, greenhouse gas concentrations, continental ice sheets and coastlines, as well as meltwater fluxes consistent with reconstructions. For more details of the model simulation see He (2011) and Liu et al. (2009).

3. Results

3.1. Core GeoB10069-3

The $\delta^{18}O_{calcite}$ of *G. ruber* from GeoB10069-3 increased by ~0.5‰ from 35 kyr BP to 20 kyr BP, consistent with the increase in global ice volume (Waelbroeck et al., 2002). $\delta^{18}O_{calcite}$ decreased by ~1.75‰ beginning at ~18 kyr BP until stabilizing at ~8 kyr BP (Fig. 3). Approximately, 1‰ of this decrease can be attributed to the global change in ice volume (Clark and Mix, 2002; Schrag et al., 2002).

Between 35–20 kyr BP, there is no significant trend in the Mg/Ca. The average Mg/Ca is 3.4 mmol/mol (25.6 ± 0.1 °C; standard error using 114 data points), with the bulk of the samples (1σ) falling between 3.3–3.6 mmol/mol (26.1–25.1 °C). The minimum value is 3.1 mmol/mol (24.4 ± 0.9 °C) and the maximum value is 3.9 mmol/mol (26.9 ± 1.1 °C). Mg/Ca values average 3.6 mmol/mol (25.9 ± 0.4 °C; standard error using 6 data points) from 20–19 kyr BP. Mg/Ca values increase during the deglaciation peaking at 4.5 mmol/mol (28.5 ± 0.3 °C; standard error using 16 data points). Mg/Ca values decrease throughout the Holocene; from 1–0 kyr BP Mg/Ca was 4.0 mmol/mol (27.2 ± 0.3 °C; standard error using 10 data points). SST estimates at GeoB10069-3 are similar to those described previously for nearby core MD98-2165 (Levi et al., 2007) (Supplementary Fig. 3). For a more detailed discussion of the GeoB10069-3 SST record, see Gibbons (2012).

The $\delta^{18}O_{sw\text{-}iv}$ reconstruction suggests several notable features. Glacial (35–20 kyr BP) and early Holocene $\delta^{18}O_{sw\text{-}iv}$ values are similar, about −0.1‰ and 0‰, respectively (Fig. 3). $\delta^{18}O_{sw\text{-}iv}$ decreased to approximately −0.2‰ by 4 kyr BP and then remained approximately constant for the remainder of the Holocene. The $\delta^{18}O_{sw\text{-}iv}$ record is, however, punctuated with millennial-scale excursions. The most pronounced events occurred during the deglaciation from 19.5 until 15 kyr BP and from ~12.5 kyr BP until 11.2 kyr BP. Smaller magnitude excursions to higher values occur during the glacial interval, from 32.5–31 kyr BP, approximately consistent with some estimates of the age of Heinrich Event 3 (Hemming, 2004), and at ~28 kyr BP.

The higher $\delta^{18}O_{sw\text{-}iv}$ values during HS1 and the Younger Dryas in Savu Basin core GeoB10069-3 corroborate the $\delta^{18}O_{sw\text{-}iv}$ reconstruction from nearby Eastern Indian Ocean site MD98-2165, and contrast with the MD01-2378 and MD98-2170 records from the Timor Sea (Figs. 1 and 3), where large excursions do not occur.

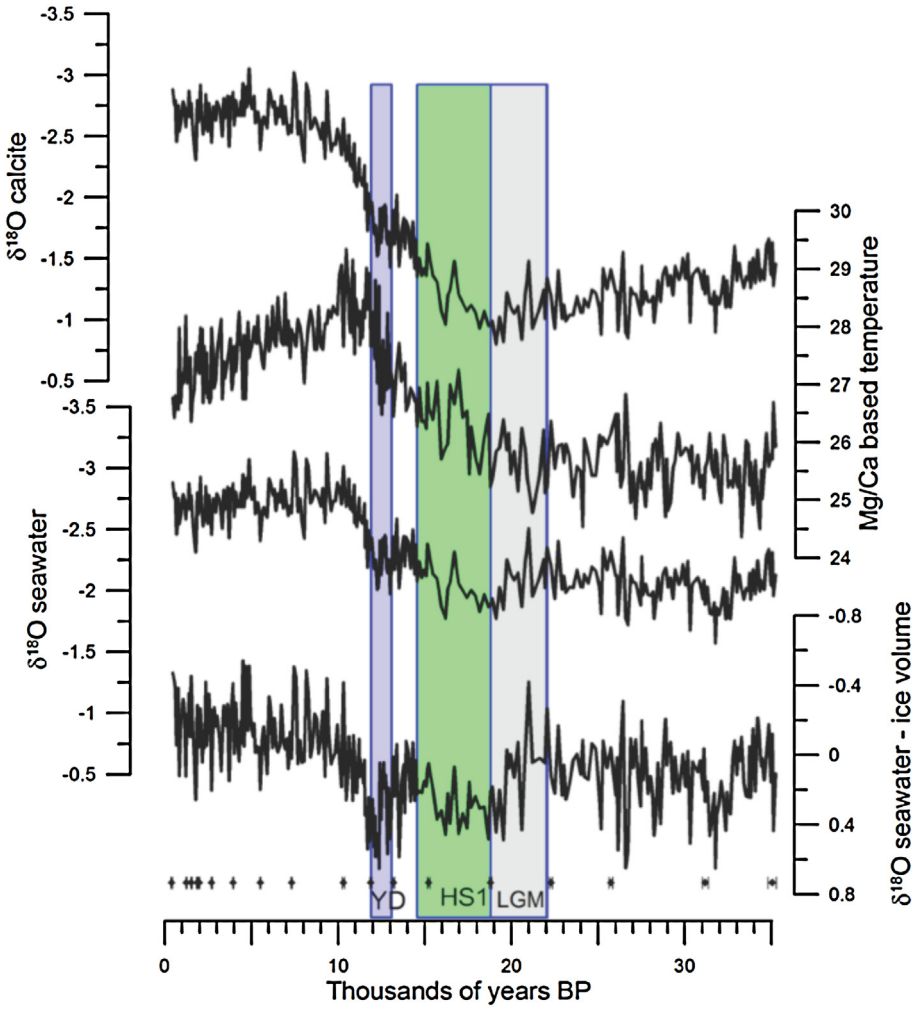

Fig. 3. Data from GeoB10069-3. Top panel is $\delta^{18}O$ of calcite. Next panel is the Mg/Ca-based temperature. These records are combined (Bemis et al., 1998) below to derive the $\delta^{18}O_{sw}$. Finally, we show the $\delta^{18}O_{sw}$ with the global ice volume effect removed. Northern hemisphere cold events (the Younger Dryas, blue and Heinrich Stadial 1, green), which correspond to periods of higher $\delta^{18}O_{sw}$, and the LGM (gray) are labeled (see also color online version).

3.2. Regional dataset

The records that we have compiled from the IPWP and Eastern Equatorial Pacific Ocean show a wide range of deglacial temperature histories (Supplementary Fig. 3). Although $\delta^{18}O_{sw\text{-}iv}$ trends also vary, most records show generally higher $\delta^{18}O_{sw\text{-}iv}$ values during the deglaciation (Fig. 4). Coherent variability among the $\delta^{18}O_{sw\text{-}iv}$ records was explored using principal component analysis. Because many of the records only span the last 20 kyr, our analysis is limited to this period, which includes only the last 1000 yr (20–19 kyr BP) of the LGM. The first principal component (PC1; Fig. 5, solid black line) explains 53% of the variance in the records and shows a coherent spatial pattern (Fig. 1).

The highest contributions to PC1 are from cores in the Eastern Equatorial Pacific (Benway et al., 2006; Koutavas et al., 2002; Lea et al., 2006) and in an Indo-Pacific geographic cluster (GeoB10069-3, GeoB10038-4 (Mohtadi et al., 2010), GeoB10029-4 (Mohtadi et al., 2010), MD98-2165 (Levi et al., 2007), MD98-2162 (Visser et al., 2003), and MD98-2181 (Stott et al., 2007)) (Fig. 1, Table 1). The similar loadings among these records suggest the dominant deglacial response in the Eastern Equatorial Pacific and Indo-Pacific is similar, with little change in the east–west gradient. Western Pacific cores MD98-2170 (Stott et al., 2007), MD98-2176 (Stott et al., 2007), and MD01-2378 (Xu et al., 2008) cluster geographically to the southeast of the Indo-Pacific cores and contribute the least to PC1; their $\delta^{18}O_{sw\text{-}iv}$ reconstructions are similar, showing relatively little variation throughout the last 20 kyr. For lack of a better term, we refer to these cores as "southern cores". The northernmost cores (MD97-2141 (Rosenthal et al., 2003) and MD01-2390 (Steinke et al., 2008)) are also minor contributors to PC1, although in both cores, there are slightly higher values that correspond to HS1 and the Younger Dryas. The reason that MD97-2141 does not contribute to the loading of PC1 is likely because $\delta^{18}O_{sw\text{-}iv}$ values are relatively low at the last glacial maximum (LGM). This may be due to lower sea level at the LGM, which allowed relatively more fresh South China Sea water than equatorial Pacific water to enter the Sulu Sea, decreasing its $\delta^{18}O_{sw}$ values (Rosenthal et al., 2003). Also, for reasons that are not clear, the duration of high values during HS1 is short compared to other cores. At MD01-2390, $\delta^{18}O_{sw\text{-}iv}$ increases throughout the Holocene, which contributes to its low loading.

The second and third principal components explain 9% and 8% of the variance, respectively, and have small amplitudes compared to PC1. Furthermore, they are much less spatially coherent than PC1 and their temporal patterns do not appear meaningful (Supplementary Figs. 4 and 5). We thus infer that these principal components are dominated by noise rather than paleoceanographic variability.

$\delta^{18}O_{sw\text{-}iv}$ data from each core were place into 500-yr intervals and averaged. The records from all cores were then averaged to produce a $\delta^{18}O_{sw\text{-}iv}$ stack with error estimates (blue dots, Fig. 5) that contains all the same major features as the

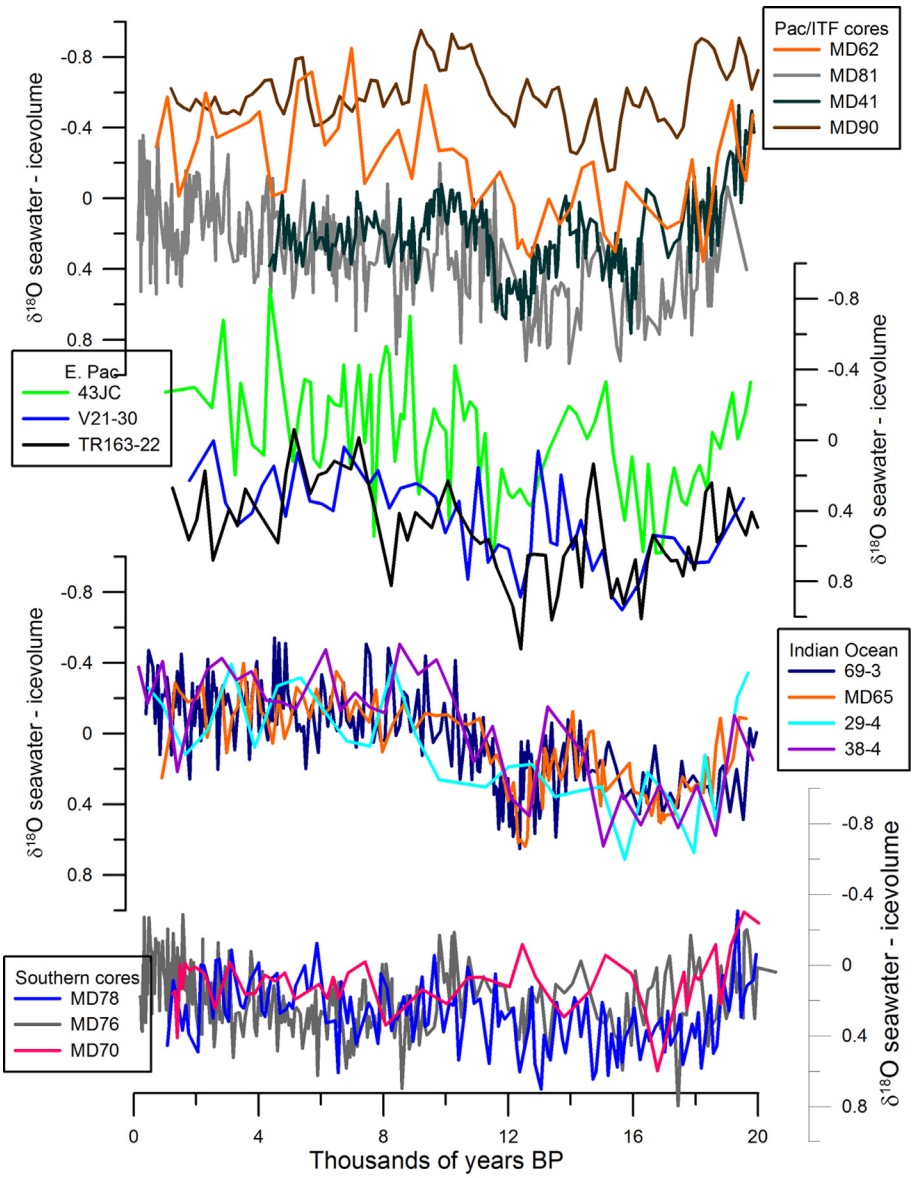

Fig. 4. $\delta^{18}O_{sw\text{-}iv}$ reconstructions from all cores used in this study. Note the generally similar LGM and late Holocene values for the $\delta^{18}O_{sw\text{-}iv}$. With the exception of the southern cores (bottom panel), many of the records show excursions to higher values during HS1 and the Younger Dryas (see also color online version).

first principal component, providing confidence that both represent important changes in tropical hydrology. Average $\delta^{18}O_{sw\text{-}iv}$ values were similar in the LGM and late Holocene, with values of approximately 0‰. As with PC1, there were two large positive excursions (>0.3‰) from 17.75–15.75 kyr BP and at 12.25 kyr BP (blue dots, Fig. 5). Regional averages for the Eastern Equatorial Pacific (ME0005A-43JC, TR163-22, and V21-30), Pacific/Indonesian Throughflow (MD97-2141, MD98-2162, MD98-2181, and MD01-2390), Indian Ocean (GeoB10029-4, GeoB10038-4, GeoB10069-3, and MD98-2165) show higher values from 17.75–15.75 kyr BP and 12.25 kyr BP whereas the southern core average (MD98-2170, MD98-2176, and MD98-2181) shows relatively little change during the past 20 kyr (Supplementary Fig. 6). Thus, the different response of the Timor Sea and Eastern Indian Ocean to North Atlantic millennial events appears to be a meaningful feature.

3.3. Model results

The transient model's precipitation responses to the increased freshwater input during the simulated HS1 (relative to the LGM, Fig. 6) and Younger Dryas (relative to the Bølling-Allerød, Supplementary Fig. 7) are similar to that in a hosing experiment on a preindustrial background (Otto-Bliesner and Brady, 2010) (Supplementary Fig. 8). Precipitation generally decreases in the western–central equatorial Pacific. In the Indian and the eastern Pacific Oceans, mean annual precipitation decreases in the northern tropics and increases in the southern tropics (Fig. 6a and Supplementary Fig. 9). This pattern is also observed over Southeast Asia and western Indonesia, with northern and southern regions experiencing less and more precipitation, respectively.

The mean annual precipitation response over the oceans leads to corresponding changes in the SSS. During the simulated HS1, SSS generally increases north of the equator and decreases south of the equator. However, the SSS response shows less spatial structure and there is a small (~0.1 psu) SSS increase over the entire tropical Indo-Pacific domain (Fig. 6, middle). For HS1, simulated evaporation–precipitation (E–P) (Supplementary Fig. 10) increases between ~10°S and ~12°N and causes overall higher SSS. Oceanic advection and mixing also smoothens out spatial structure evident in the precipitation and E–P anomaly patterns, thus contributing to a tropical wide SSS increase. SSS increases are restricted to the

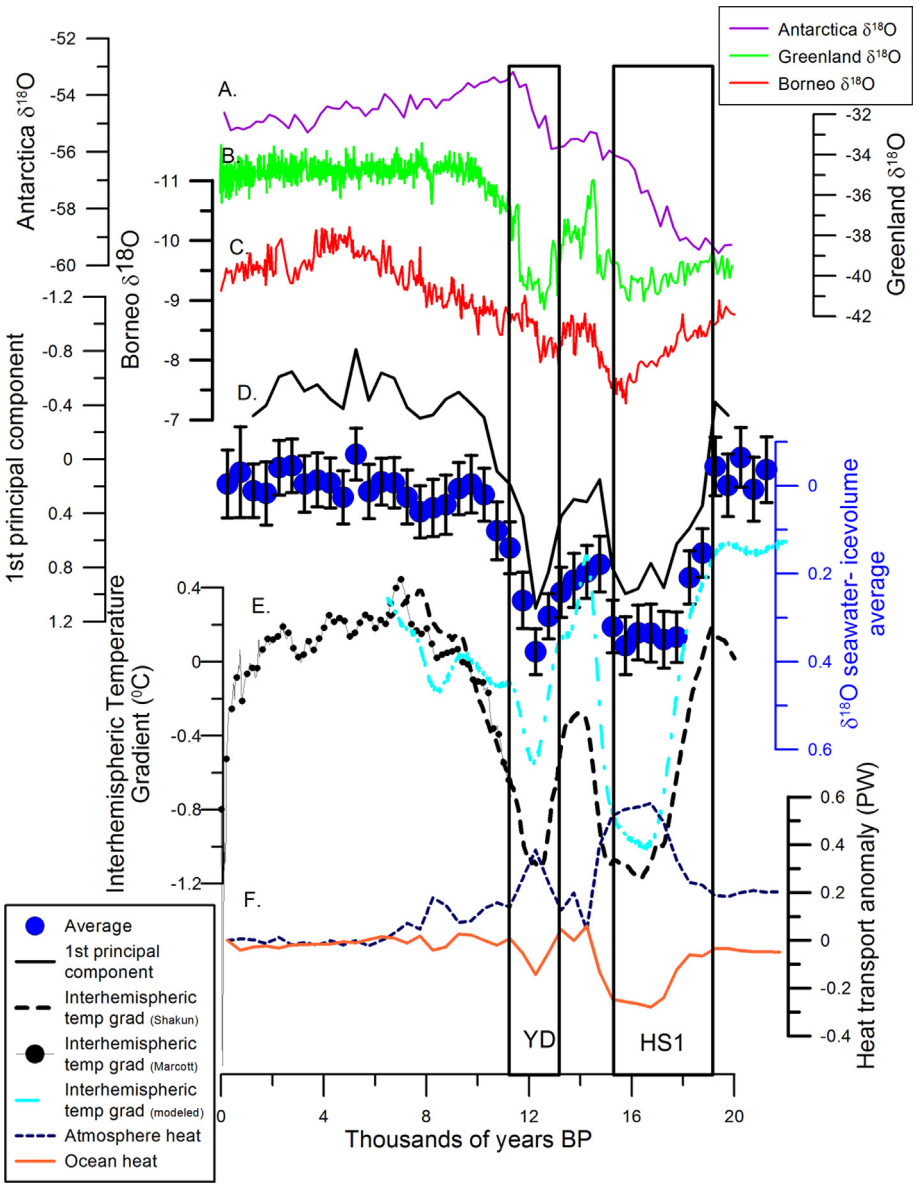

Fig. 5. A comparison of climate records: (A) δ^{18}O from Dome Fuji (Kawamura et al., 2007) (Antarctica). (B) GISP δ^{18}O (Greenland) (Grootes and Stuiver, 1997). (C) δ^{18}O of Borneo speleothems (Partin et al., 2007), with ice volume removed. (D) PC1 of all $\delta^{18}O_{sw\text{-}iv}$ records included in this study (see Table 1). Dots (blue) are an average of $\delta^{18}O_{sw\text{-}iv}$ records (error bars are 1-sigma). PC1 and the average were calculated at a 500-year resolution (see supplementary discussion). (E) Derived (black dashed line) and modeled (cyan dash–dot–dashed line) interhemispheric temperature gradients (Shakun et al., 2012) from the deglaciation and the derived Holocene interhemispheric temperature gradient (black dots) (Marcott et al., 2013). (F) Model-derived changes in heat transport for the ocean (blue dashed line) and atmosphere (orange line) (figure caption refers to color online figure).

northeastern tropical Pacific (where our cores are located) and the IPWP during the simulated YD (Supplementary Fig. 8).

4. Discussion

4.1. Robustness of the $\delta^{18}O_{sw}$ proxy

Reconstructions of $\delta^{18}O_{sw}$ can be used to infer past hydrologic changes. The $\delta^{18}O_{sw}$ and SSS usually have a positive linear relationship as both quantities are similarly influenced by evaporation and precipitation; higher $\delta^{18}O_{sw}$ values generally correspond to saltier conditions. However, the relationship varies by region and has likely varied in the past. Thus $\delta^{18}O_{sw}$ is not a simple paleosalinity proxy (LeGrande and Schmidt, 2011) and a direct conversion to salinity is not appropriate.

Some studies argue that Mg/Ca-based sea surface temperature (SST) estimates, and therefore $\delta^{18}O_{sw}$ estimates, may be biased in regions of surface salinities greater than 35 (Arbuszewski et al., 2010). All the records discussed in this study, including our new record, are from regions where today mean annual salinity is less than 35. Furthermore, in each region, $\delta^{18}O_{sw}$ is correlated with SSS and core-top data (Fig. 2) fall along the trend established by the seawater data (Fig. 7 and supplementary discussion). The major $\delta^{18}O_{sw}$ features we discuss are also present in first principal component of the $\delta^{18}O_{calcite}$ (minus global ice volume) records (Fig. 8), suggesting that these changes are robust against potential errors in the Mg/Ca–SST relationship.

4.2. IPWP hydrologic change

Higher $\delta^{18}O_{sw}$ values in the eastern Indian Ocean during HS1 and the Younger Dryas are consistent with inferred reduced runoff based on median grain size changes in a sediment core off the south coast of Java (Mohtadi et al., 2011). However, an excess ^{232}Th

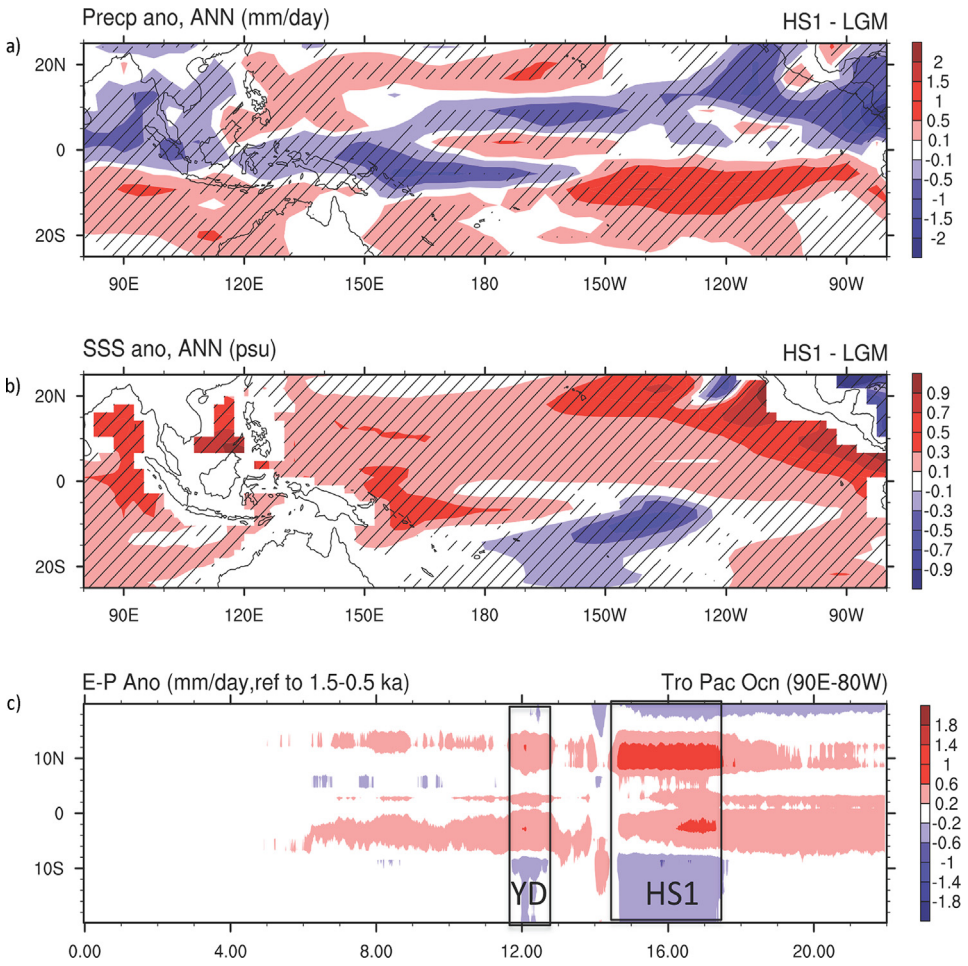

Fig. 6. Results from a transient run of the National Center for Atmospheric Research's Community Climate System Model version 3. Annual precipitation differences (top, a) and sea surface salinity difference (middle, b) between the simulated HS1 and the LGM. Zonal mean evaporation minus precipitation for the entire transient run (22-0 kyr BP) averaged zonally from the central tropical Indian Ocean to the eastern tropical Pacific (90E–80W) (bottom, c). In (a) and (b), gray areas with solid contours are positive anomalies; white areas with dashed contours are negative anomalies (see also color online figure; in color figure hashed zones are significant at the 99.9% level).

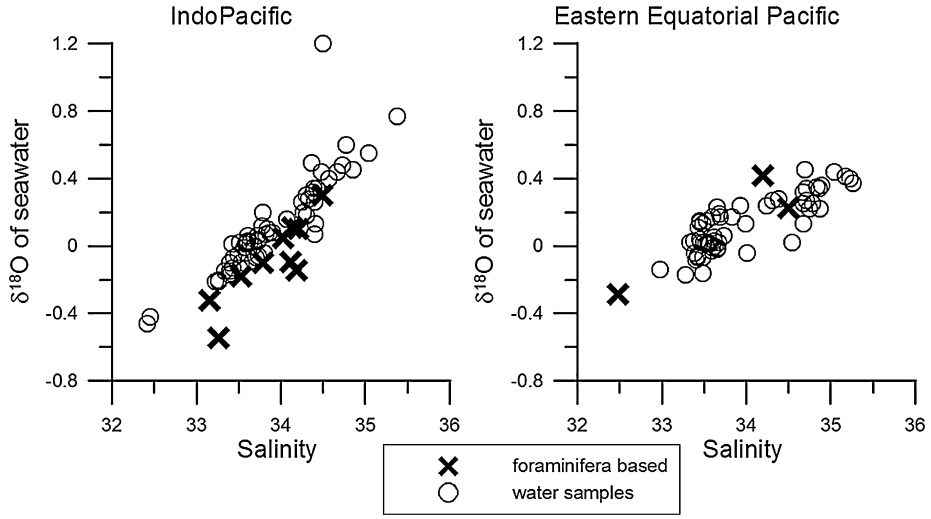

Fig. 7. Foraminifera-based reconstructed "modern" $\delta^{18}O_{sw}$ estimates plotted against modern WOA05 salinity data (Antonov et al., 2006). Modern water $\delta^{18}O_{sw}$ and salinity data (LeGrande and Schmidt, 2006) are also shown. The Indo-Pacific plot includes all water data from 90°E–140°E and 10°N–10°S. The Indo-Pacific foraminifera-based data are from cores GeoB10029-4, GeoB10038-4, GeoB10069-3, MD98-2162, MD98-2165, MD98-2170, MD98-2176, MD98-2181, MD01-2378, and MD01-2390. The Eastern Equatorial Pacific plot includes data from 90°W to 100°W and 11°N to 10°S. The Eastern Equatorial Pacific foraminifera-based data are from ME0005A-43JC, TR163-22, and V21-30. All water samples are from 100 m or above and most are from the surface. Additionally, only actual water data are used, not the gridded product. For the Indo-Pacific samples, the slope for the foraminifera-based line is 0.48 ($R^2 = 0.76$) and for the water samples it is 0.44 ($R^2 = 0.79$). For the Eastern Equatorial Pacific the slope for the modern is 0.22 ($R^2 = 0.70$) and the reconstructed $\delta^{18}O_{sw}$ values tend to fall within the scatter of the data. All cores are from locations that are from relatively fresh locations, and thus we make no correction for salinity to the Mg/Ca (Arbuszewski et al., 2010).

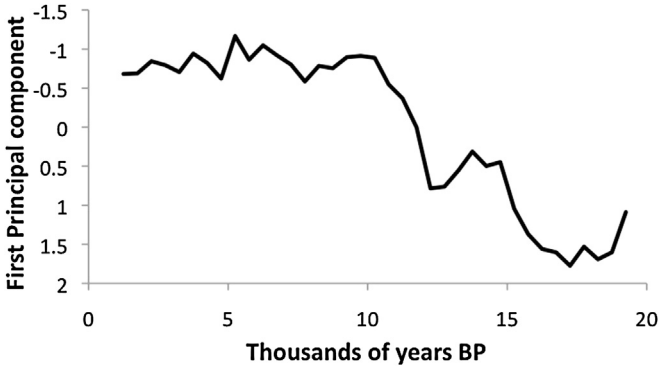

Fig. 8. The first principal component of $\delta^{18}O_{calcite}$, with global ice volume removed. This principal component explains 75% of the variance, and exhibits positive excursions during HS1 and the YD, suggesting that the $\delta^{18}O_{sw\text{-}iv}$ records are not an artifact of the Mg/Ca-based SSTs.

record from a marine core in the Flores Sea suggests an increase in runoff during the HS1 event (Muller et al., 2012), and speleothems from Flores suggest an increase in precipitation during the Younger Dryas (Griffiths et al., 2009).

The observation that in the transient simulation, salinity increases during North Atlantic abrupt cold events even in many areas of simulated increased precipitation (Fig. 6 and Supplementary Fig. 7) helps reconcile proxy evidence for increased precipitation on Flores with higher $\delta^{18}O_{sw}$ in nearby cores. The southern Indonesian sites (MD98-2170, MD98-2176, and MD01-2378) that show little change over the course of the deglaciation are in a region where the model simulation suggests increased precipitation during HS1 and the YD, but little or no change in salinity, consistent with the interpretation that $\delta^{18}O_{sw}$ primarily reflects changes in salinity. Thus, the increases in salinity and $\delta^{18}O_{sw}$ are not inconsistent with hydrologic changes during North Atlantic cold events as indicated by terrestrial precipitation and runoff proxies.

The higher $\delta^{18}O$ values during Heinrich events in Borneo speleothems have been attributed to reduced local rainfall caused by a southward displacement of the ITCZ (Partin et al., 2007) consistent with sensitivity studies using an isotope-enabled global coupled model showing that rainfall abundance is the most important factor controlling precipitation $\delta^{18}O$ at Borneo (Lewis et al., 2010). The global ice volume-corrected $\delta^{18}O$ from the Borneo speleothem record reveals a 0.5‰ increase during the early Younger Dryas (Fig. 5), also likely due to a southward displacement of the ITCZ. Moreover, a new $\delta^{18}O$ record from a speleothem from northern Australia suggests enhanced austral summer Indo-Australian monsoon precipitation during the Heinrich Stadial and the Younger Dryas, also consistent with a southward migration of the ITCZ–monsoon system (Denniston et al., 2013).

The global ice volume-corrected speleothem $\delta^{18}O$ from Borneo (Partin et al., 2007) has higher LGM values than modern, contrasting with $\delta^{18}O_{sw}$ records from the "Pacific/ITF" cluster (Fig. 4). However, as already noted, $\delta^{18}O_{sw\text{-}iv}$ variations reflect hydrologic changes on a larger regional scale than do the terrestrial records, and so differences between these records during the LGM may also result from decoupling between local precipitation and larger scale salinity changes that are mixed/advected by ocean currents.

A recent data compilation and modeling study (DiNezio and Tierney, 2013) suggests that the exposure of the Sunda Shelf contributed significantly to regional drying during the LGM, including drying over Borneo. Although the authors also evaluated $\delta^{18}O_{sw\text{-}iv}$ records, our finding of no significant difference between LGM and modern $\delta^{18}O_{sw\text{-}iv}$ values (Fig. 5) seem to contrast with their conclusion that much of the IPWP was fresher during the LGM. However, the focus of their study was the LGM rather than millennial variability, which enabled them to include low resolution, poorly dated records, including several from the western equatorial Pacific that we excluded in our study, and most of the fresh IPWP they describe is outside our study area (the Indonesian Seas/eastern Indian Ocean) or where we also infer lower $\delta^{18}O_{sw\text{-}iv}$ (the South China Sea). Indeed, the pattern of LGM $\delta^{18}O_{sw\text{-}iv}$ anomalies in our study area is nearly identical to DiNezio and Tierney (2013)'s fresh/salty pattern with most of the data in both studies suggesting no change within the Indonesian Seas. Nevertheless, there is a discrepancy in the Timor Sea (see Supplementary Fig. 1 for location map), where their use of time slice data (21.5-18 kyr BP) from (Xu et al., 2010) that includes the oldest portion of HS1 contributes to inferred salty conditions in the region. Continuous records from the region, MD01-2378 (Xu et al., 2010), MD98-2170 (Stott et al., 2002; Stott et al., 2007), and SO18460 (Holbourn et al., 2011), do not have significantly higher $\delta^{18}O_{sw\text{-}iv}$ values during the LGM (Fig. 4 and Supplementary Fig. 6), and we classify this as a region of little or no change. Furthermore, as we discuss in Section 4.4, our finding of little LGM-Holocene $\delta^{18}O_{sw\text{-}iv}$ change is consistent with a small LGM-Holocene difference in the interhemispheric temperature gradient.

4.3. The role of ENSO-like variability

It has been hypothesized that if the tropical Pacific becomes "locked" in either a permanent El Niño or La Niña-like state, the resulting teleconnections could affect global climate and produce both millennial and glacial/interglacial scale climate variability (Clement et al., 1999). Several authors have attributed past changes in tropical $\delta^{18}O_{sw}$ to ENSO-like variability, as inferred from the east–west tropical Pacific temperature gradient (Levi et al., 2007; Rosenthal et al., 2003; Stott et al., 2002). There is no clear evidence, however, to support large ENSO-like changes during either the LGM or during the deglaciation (DiNezio et al., 2011; Leduc et al., 2009; Liu et al., 2005; Rosenthal and Broccoli, 2004). Because ENSO variability is also reflected in east–west tropical precipitation gradients, we can use our more complete $\delta^{18}O_{sw}$ dataset to evaluate whether there is evidence of ENSO-like variability.

The Eastern Equatorial core sites used in this study cover nearly the entire latitudinal span where precipitation increases during an El Niño event (e.g. de Garidel-Thoron et al., 2007) and thus provide a sufficiently large sample to assess the Eastern Equatorial response to ENSO-like changes. During an El Niño event, the core sites in the IPWP are in a region where precipitation decreases (de Garidel-Thoron et al., 2007). Thus, at our study sites, ENSO-like changes would result in opposite precipitation anomalies in the eastern and western tropical Pacific. To evaluate the plausibility of the ENSO-like forcing, we plot the $\delta^{18}O_{sw\text{-}iv}$ anomalies relative to present at each core site for 1000-yr long time slices centered within the LGM, HS1, and Younger Dryas (Fig. 9). These results suggest that Eastern Equatorial Pacific and Indo-Pacific $\delta^{18}O_{sw\text{-}iv}$ values increase by approximately the same amount during HS1 and the Younger Dryas; LGM values are similar to modern. Thus, the east–west Pacific $\delta^{18}O_{sw}$ gradient remained approximately constant through time, with the corollary that ENSO analogues do not drive millennial-scale changes in the deglacial hydrology of our study regions, consistent with a previous inference based on only three sites (Leduc et al., 2009). However, at present, the slope between $\delta^{18}O_{sw}$ and salinity is shallower in the east than the west (Fig. 7), suggesting that if there were similar differences in slope between the two regions in the past, we might not discern subtle changes in the east–west salinity gradients. Nevertheless, our results suggest that if east–west gradient changes occurred, they were minor compared to the coherent variations of the same sign, thus our data do not support a significant role for an ENSO-like mechanism on glacial–interglacial time scales, or during millennial events of the last deglaciation (Clement et al., 1999).

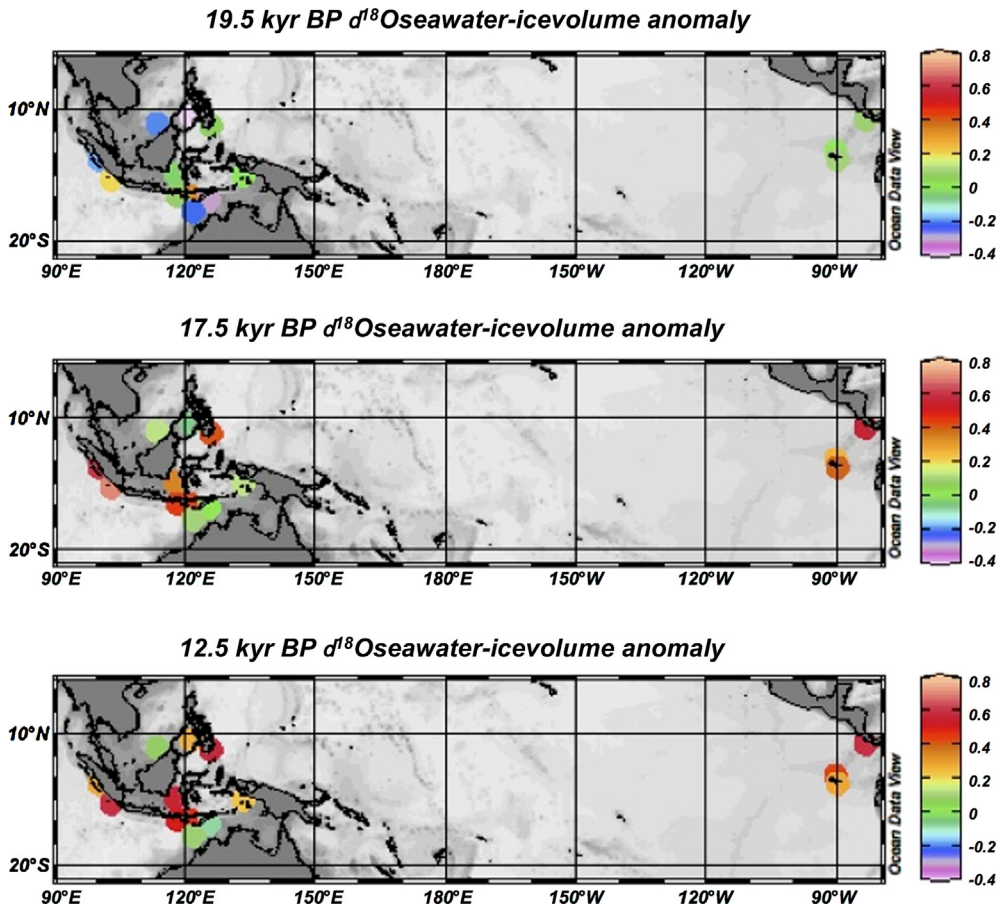

Fig. 9. $\delta^{18}O_{sw\text{-}iv}$ anomalies relative to present. All panels are averages of 1000 years. Top panel is centered on 19.5 kyr BP, middle panel is centered on 17.5 kyr BP, and bottom panel is centered on 12.5 kyr BP (see also color online version; see supplementary discussion for details on anomaly calculation).

4.4. Hydrologic variability and the interhemispheric temperature gradient

Our hydrologic reconstruction, specifically PC1, does not parallel either northern or southern high-latitude temperature variability (Fig. 5). The transient NCAR GCM simulation and other model sensitivity studies suggest that deglacial melt water pulses to the Atlantic Ocean reduce the Atlantic Meridional Overturning Circulation. As a consequence, northward oceanic heat transport is reduced (Fig. 5), giving rise to a reduction in the interhemispheric SST gradient (Shakun et al., 2012).

Our hydrologic reconstruction (PC1) shows a strong relationship with changes in the reconstructed deglacial interhemispheric temperature gradient (Shakun et al., 2012), which spans the interval 19.75 kyr BP to 6.75 kyr BP ($r^2 = 0.79$, $p \ll 0.001$) (Fig. 5). To extend the comparison into the late Holocene, we follow Shakun et al. (2012) and group Holocene temperature reconstructions from Marcott et al. (2013) into Northern and Southern hemisphere bins (see supplemental discussion). We find a statistically significant correlation between PC1 and the Holocene interhemispheric temperature gradient, which spans the interval from 1.25 kyr BP to 11.25 kyr BP ($r^2 = 0.62$, $p \ll 0.001$). We combine data from Marcott et al. (2013) and Shakun et al. (2012) by averaging the two data sets where they overlap. The correlation between PC1 and the full-length interhemispheric gradient (19.75 kyr BP to 1.25 kyr BP) is also statistically significant ($r^2 = 0.87$, $p \ll 0.001$).

At the LGM, the interhemispheric temperature gradient was similar to the mid-Holocene gradient. LGM and Holocene values of the $\delta^{18}O_{sw\text{-}iv}$-based hydrologic reconstructions (PC1 and the average value) are indistinguishable. During the deglaciation, dramatic changes occur in both the inferred hydrology and interhemispheric temperature gradient. The changes in PC1 during HS1 and the Younger Dryas, which are primarily driven by higher values in the Eastern Equatorial Pacific (ME0005A-43JC, TR163-22, and V21-30) and center of the IPWP (GeoB10029-4, GeoB10038-4, GeoB10069-3, MD98-2162, MD98-2165, and MD98-2181) (Fig. 1), correspond to a smaller interhemispheric temperature gradient.

At present, the mean position of the ITCZ is biased towards the northern hemisphere; on average, its position is north of the equator. As a result, the mean position of the rising branch of the Hadley Cell is north of the equator resulting in the southward atmospheric heat transport across the equator (Broccoli et al., 2006). Simulations with global coupled climate models suggest that the mean position of the ITCZ is sensitive to the interhemispheric temperature gradient (Broccoli et al., 2006; Chiang and Friedman, 2012).

Our results, showing that large-scale variations in tropical hydrology, in part reflecting ITCZ movement, more closely parallel the interhemispheric temperature gradient than either northern or southern hemisphere temperature variations, suggest that the observed response of tropical hydrology to northern hemisphere cold events is due to the influence of the interhemispheric temperature gradient. This result is consistent with a recent study by Donohoe et al. (2013) showing a strong relationship between the interhemispheric temperature gradient and the ITCZ position in the modern seasonal cycle as well as in model studies of past climates (LGM and mid-Holocene) and doubled CO_2 simulations. The authors also demonstrate that the mean position of the ITCZ is rarely realized

due to its regular seasonal north/south shifts, and its northern position occurs because the ITCZ spends more time in the northern hemisphere.

The transient model simulation shows the resulting atmospheric rearrangement partially compensates for the reduced oceanic heat transport (Fig. 5), consistent with modern observations and other modeling studies (Zhang et al., 2010). Studies explicitly examining the relationship between the ITCZ and atmosphere heat transport have demonstrated that a southwardly displaced ITCZ leads to more northward atmospheric heat transport (Donohoe et al., 2013; Marshall et al., 2013). Collectively, these results suggest the tropical atmosphere responds to, and to some extent compensates for, changes in the Atlantic Meridional Overturning Circulation.

4.5. Holocene trends

Numerous regional records show substantial Holocene hydrologic variability (e.g. Griffiths et al., 2009; Partin et al., 2007; Wang et al., 2005). The interhemispheric temperature gradient based on data compiled by Marcott et al. (2013) shows relatively little change between ~9 and 5 kyr PB, but shows a decrease from ~5 kyr PB to the late Holocene, contrasting with PC1, which shows almost no change. We suggest that the reason for this lack of coherence compared to the deglaciation relates to the relative magnitudes of the interhemispheric temperature gradient during North Atlantic cold events and the late Holocene. During North Atlantic cold events, one of the main effects of the large interhemispheric temperature gradients was to shift mean annual precipitation southward. By contrast, factors in addition to the smaller and more gradual increase in the interhemispheric temperature gradient influenced precipitation patterns and oceanic salinity during the last 5 kyr. For example, the redistribution of precipitation between the land and the oceans and differences in basin–basin oceanic vapor transport may have influenced Pacific salinities (Oppo et al., 2007). Furthermore changes in the Walker circulation may have induced Indian and Pacific spatial patterns (e.g. Conroy et al., 2008; Tierney et al., 2012). A related reason for the lack of a late Holocene trend in PC1 is that the $\delta^{18}O_{sw\text{-}iv}$ signals during this interval are small compared to the errors. Whereas records published by Stott et al. (2004) suggested mid-late Holocene freshening in the western Pacific, our compilation includes many records without this trend (Fig. 4).

5. Summary and conclusions

Our data suggest that past variations in $\delta^{18}O_{sw\text{-}iv}$ of the tropical Pacific generally reflect salinity changes. Further, we reconstruct the dominant mode of Indo-Pacific and Eastern Equatorial Pacific $\delta^{18}O_{sw\text{-}iv}$. LGM and Holocene values are similar and there are large positive excursions during HS1 and the Younger Dryas. The dominant $\delta^{18}O_{sw\text{-}iv}$ mode does not simply follow Northern Hemisphere temperature; rather, it is more closely tied to the interhemispheric temperature gradient ($r^2 = 0.87$). A transient model simulation suggests that during these Northern Hemisphere cold events, precipitation increased north of the equator and decreased south of the equator, corresponding to a southward shift of the anomalous ITCZ rainfall. This southward shift leads to increased atmospheric heat transport towards the Northern Hemisphere, suggesting that the tropical atmosphere not only responds to, but to some extent compensates for, changes in the Atlantic Meridional Overturning Circulation. The modeled tropical hydrologic changes during Northern Hemisphere cold events cause increases in the salinity of much of the IPWP and in the eastern tropical Pacific, even in some areas where precipitation increases. Thus, we suggest that $\delta^{18}O_{sw\text{-}iv}$ generally reflects large-scale changes in the hydrologic cycle, an interpretation that is consistent with modeling results and reconciles apparent conflicts with terrestrial data. Future work with isotope-enabled Earth Systems Models will allow us to more fully explore the source of the differences between terrestrial and marine archives.

Acknowledgements

We thank O. Marchal for assistance with principal component analysis and error analysis, D. McGee for helpful discussions, and anonymous reviewers for helpful comments. This work was funded by the National Science Foundation; the Ocean and Climate Change Institute and the Academic Programs Office at Woods Hole Oceanographic Institution; BMBF (PABESIA); and DFG (He 3412/15-1)

Appendix A. Supplementary material

Supplementary material related to this article can be found online at http://dx.doi.org/10.1016/j.epsl.2013.11.032.

References

Antonov, J.I., Locarnini, R.A., Boyer, T.P., Garcia, H.E., 2006. World Ocean Atlas. 2005, vol. 2: Salinity, NOAA Atlas NESDIS 62.

Arbuszewski, J., de Menocal, P.B., Kaplan, A., Farmer, E.C., 2010. On the fidelity of shell-derived $\delta^{18}O$ sea water estimates. Earth Planet. Sci. Lett. 300 (3–4), 185–196. http://dx.doi.org/10.1016/j.epsl.2010.10.035.

Bemis, B.E., Spero, H.J., Bijma, J., Lea, D.W., 1998. Reevaluation of the oxygen isotopic composition of planktonic foraminifera: Experimental results and revised paleotemperature equations. Paleoceanography 13 (2), 150–160.

Benway, H.M., Mix, A.C., Haley, B.A., Klinkhammer, G.P., 2006. Eastern Pacific Warm Pool paleosalinity and climate variability: 0–30 kyr. Paleoceanography 21 (3), Pa3008. http://dx.doi.org/10.1029/2005pa001208.

Bond, G., Heinrich, H., Broecker, W., Labeyrie, L., Mcmanus, J., Andrews, J., Huon, S., Jantschik, R., Clasen, S., Simet, C., Tedesco, K., Klas, M., Bonani, G., Ivy, S., 1992. Evidence for massive discharges of icebergs into the North-Atlantic Ocean during the Last Glacial Period. Nature 360 (6401), 245–249.

Bond, G., Broecker, W., Johnsen, S., Mcmanus, J., Labeyrie, L., Jouzel, J., Bonani, G., 1993. Correlations between climate records from North-Atlantic sediments and Greenland ice. Nature 365 (6442), 143–147.

Boyle, E.A., Keigwin, L.D., 1985/1986. Comparison of Atlantic and Pacific paleochemical records for the last 215,000 years – changes in deep ocean circulation and chemical inventories. Earth Planet. Sci. Lett. 76 (1–2), 135–150.

Broccoli, A.J., Dahl, K.A., Stouffer, R.J., 2006. Response of the ITCZ to Northern Hemisphere cooling. Geophys. Res. Lett. 33 (1), L01702. http://dx.doi.org/10.1029/2005gl024546.

Broecker, W.S., 1991. The Great Ocean conveyor. Oceanography 4 (2), 79–89.

Broecker, W.S., 2006. Was the younger dryas triggered by a flood? Science 312 (5777), 1146–1148. http://dx.doi.org/10.1126/Science.1123253.

Chiang, J.C., Friedman, A.R., 2012. Extratropical cooling, interhemispheric thermal gradients, and tropical climate change. Annu. Rev. Earth Planet. Sci. 40, 383–412.

Clark, P.U., Mix, A.C., 2002. Ice sheets and sea level of the Last Glacial Maximum. Quat. Sci. Rev. 21 (1–3), 1–7. http://dx.doi.org/10.1016/S0277-3791(01)00118-4.

Clement, A.C., Seager, R., Cane, M.A., 1999. Orbital controls on the El Niño/Southern Oscillation and the tropical climate. Paleoceanography 14 (4), 441–456.

Conroy, J.L., Overpeck, J.T., Cole, J.E., Shanahan, T.M., Steinitz-Kannan, M., 2008. Holocene changes in eastern tropical Pacific climate inferred from a Galapagos lake sediment record. Quat. Sci. Rev. 27 (11), 1166–1180.

de Garidel-Thoron, T., Rosenthal, Y., Beaufort, L., Bard, E., Sonzogni, C., Mix, A.C., 2007. A multiproxy assessment of the western equatorial Pacific hydrography during the last 30 kyr. Paleoceanography 22 (3), Pa3204. http://dx.doi.org/10.1029/2006pa001269.

Denniston, R.F., Wyrwoll, K.-H., Asmerom, Y., Polyak, V.J., Humphreys, W.F., Cugley, J., Woods, D., LaPointe, Z., Peota, J., Greaves, E., 2013. North Atlantic forcing of millennial-scale Indo-Australian monsoon dynamics during the Last Glacial period. Quat. Sci. Rev. 72, 159–168.

DiNezio, P.N., Clement, A., Vecchi, G.A., Soden, B., Broccoli, A.J., Otto-Bliesner, B.L., Braconnot, P., 2011. The response of the Walker circulation to Last Glacial Maximum forcing: Implications for detection in proxies. Paleoceanography 26, Pa3217. http://dx.doi.org/10.1029/2010pa002083.

DiNezio, P.N., Tierney, J.E., 2013. The effect of sea level on glacial Indo-Pacific climate. Nat. Geosci. 6, 485–491. http://dx.doi.org/10.1038/NGEO1823.

Ding, X., Guichard, F., Bassinot, F., Labeyrie, L., Nianqiao, F., 2002. Evolution of heat transport pathways in the Indonesian Archipelago during last deglaciation. Chin. Sci. Bull. 47 (22), 1912–1917.

Donohoe, A., Marshall, J., Ferreira, D., Mcgee, D., 2013. The relationship between ITCZ location and cross equatorial atmospheric heat transport; from the seasonal cycle to the Last Glacial Maximum. J. Climate 26, 3597–3618.

Gibbons, F.T., 2012. The Centennial and Millennial Variability of the Indo-Pacific Warm Pool and the Indonesian Throughflow. Massachusetts Institute of Technology and the Woods Hole Oceanographic Institution, Cambridge/Woods Hole. 142 pp.

Griffiths, M.L., Drysdale, R.N., Gagan, M.K., Zhao, J.X., Ayliffe, L.K., Hellstrom, J.C., Hantoro, W.S., Frisia, S., Feng, Y.X., Cartwright, I., Pierre, E.S., Fischer, M.J., Suwargadi, B.W., 2009. Increasing Australian–Indonesian monsoon rainfall linked to early Holocene sea-level rise. Nat. Geosci. 2 (9), 636–639. http://dx.doi.org/10.1038/Ngeo605.

Grootes, P.M., Stuiver, M., 1997. Oxygen 18/16 variability in Greenland snow and ice with 10^3 to 10^5-year time resolution. J. Geophys. Res. 102, 26455–26470.

Hall, I.R., Moran, S.B., Zahn, R., Knutz, P.C., Shen, C.C., Edwards, R.L., 2006. Accelerated drawdown of meridional overturning in the late-glacial Atlantic triggered by transient pre-H event freshwater perturbation. Geophys. Res. Lett. 33 (16), L16616. http://dx.doi.org/10.1029/2006gl026239.

He, F., 2011. Simulating Transient Climate Evolution of the Last Deglaciation with CCSM3. University of Wisconsin–Madison. 171 pp.

Heinrich, H., 1988. Origin and consequences of cyclic ice rafting in the Northeast Atlantic-Ocean during the past 130,000 years. Quat. Res. 29 (2), 142–152.

Hemming, S.R., 2004. Heinrich events: Massive late pleistocene detritus layers of the North Atlantic and their global climate imprint. Rev. Geophys. 42 (1), Rg1005. http://dx.doi.org/10.1029/2003rg000128.

Holbourn, A., Kuhnt, W., Xu, J., 2011. Indonesian Throughflow Variability During the Last 140 ka: The Timor Sea Outflow. Geological Society, London.

Jolliffe, I.T., 2002. Principal Component Analysis, 2nd edition. Springer.

Kawamura, K., Parrenin, F., Lisiecki, L., Uemura, R., Vimeux, F., Severinghaus, J.P., Hutterli, M.A., Nakazawa, T., Aoki, S., Jouzel, J., Raymo, M.E., Matsumoto, K., Nakata, H., Motoyama, H., Fujita, S., Goto-Azuma, K., Fujii, Y., Watanabe, O., 2007. Northern Hemisphere forcing of climatic cycles in Antarctica over the past 360,000 years. Nature 448, 912–916. http://dx.doi.org/10.1038/nature06015.

Kiefer, T., Kienast, M., 2005. Patterns of deglacial warming in the Pacific Ocean: a review with emphasis on the time interval of Heinrich event 1. Quat. Sci. Rev. 24, 1063–1081. http://dx.doi.org/10.1016/j.quascirev.2004.02.021.

Koutavas, A., Lynch-Stieglitz, J., Marchitto, T.M., Sachs, J.P., 2002. El Niño-like pattern in ice age tropical Pacific sea surface temperature. Science 297 (5579), 226–230.

Lea, D.W., Pak, D.K., Spero, H.J., 2000. Climate impact of late quaternary equatorial Pacific sea surface temperature variations. Science 289 (5485), 1719–1724.

Lea, D.W., Pak, D.K., Belanger, C.L., Spero, H.J., Hall, M.A., Shackleton, N.J., 2006. Paleoclimate history of Galapagos surface waters over the last 135,000 yr. Quat. Sci. Rev. 25 (11–12), 1152–1167. http://dx.doi.org/10.1016/j.quascirev.2005.11.010.

Leduc, G., Vidal, L., Tachikawa, K., Bard, E., 2009. ITCZ rather than ENSO signature for abrupt climate changes across the tropical Pacific?. Quat. Res. 72 (1), 123–131. http://dx.doi.org/10.1016/J.Yqres.2009.03.006.

LeGrande, A.N., Schmidt, G.A., 2006. Global gridded data set of the oxygen isotopic composition in seawater. Geophys. Res. Lett. 33 (12), L12604. http://dx.doi.org/10.1029/2006GL026011.

LeGrande, A.N., Schmidt, G.A., 2011. Water isotopologues as a quantitative paleosalinity proxy. Paleoceanography 26, Pa3225. http://dx.doi.org/10.1029/2010pa002043.

Levi, C., Labeyrie, L., Bassinot, F., Guichard, F., Cortijo, E., Waelbroeck, C., Caillon, N., Duprat, J., de Garidel-Thoron, T., Elderfield, H., 2007. Low-latitude hydrological cycle and rapid climate changes during the last deglaciation. Geochem. Geophys. Geosyst. 8 (5), Q05N12. http://dx.doi.org/10.1029/2006GC001514.

Lewis, S.C., LeGrande, A.N., Kelley, M., Schmidt, G.A., 2010. Water vapour source impacts on oxygen isotope variability in tropical precipitation during Heinrich events. Clim. Past 6 (3), 325–343. http://dx.doi.org/10.5194/Cp-6-325-2010.

Linsley, B.K., Rosenthal, Y., Oppo, D.W., 2010. Holocene evolution of the Indonesian throughflow and the western Pacific warm pool. Nat. Geosci. 3, 578–583.

Liu, Z., Vavrus, S., He, F., Wen, N., Zhong, Y., 2005. Rethinking tropical ocean response to global warming: the enhanced equatorial warming. J. Climate 18 (22), 4684–4700.

Liu, Z., Otto-Bliesner, B.L., He, F., Brady, E.C., Tomas, R., Clark, P.U., Carlson, A.E., Lynch-Stieglitz, J., Curry, W., Brook, E., Erickson, D., Jacob, R., Kutzbach, J., Cheng, J., 2009. Transient simulation of last deglaciation with a new mechanism for Bølling–Allerød warming. Science 325 (5938), 310–314. http://dx.doi.org/10.1126/science.1171041.

Locarnini, R.A., Mishonov, A.V., Antonov, J.I., Boyer, T.P., Garcia, H.E., 2006. World Ocean Atlas. 2005, vol. 1: Temperature, NOAA Atlas NESDIS 61.

Marcott, S.A., Shakun, J.D., Clark, P.U., Mix, A.C., 2013. A reconstruction of regional and global temperature for the past 11,300 years. Science 339 (6124), 1198–1201.

Marshall, J., Donohoe, A., Ferreira, D., McGee, D., 2013. The ocean's role in setting the mean position of the Inter-Tropical Convergence Zone. Clim. Dyn.. http://dx.doi.org/10.1007/s00382-013-1767-z.

McManus, J.F., Francois, R., Gherardi, J.M., Keigwin, L.D., Brown-Leger, S., 2004. Collapse and rapid resumption of Atlantic meridional circulation linked to deglacial climate changes. Nature 428 (6985), 834–837. http://dx.doi.org/10.1038/Nature02494.

Mohtadi, M., Steinke, S., Lückge, A., Groeneveld, J., Hathorne, E.C., 2010. Glacial to Holocene surface hydrography of the tropical eastern Indian Ocean. Earth Planet. Sci. Lett. 292, 89–97. http://dx.doi.org/10.1016/j.epsl.2010.01.024.

Mohtadi, M., Oppo, D.W., Steinke, S., Stuut, J.B.W., De Pol-Holz, R., Hebbeln, D., Luckge, A., 2011. Glacial to Holocene swings of the Australian-Indonesian monsoon. Nat. Geosci. 4 (8), 540–544. http://dx.doi.org/10.1038/Ngeo1209.

Muller, J., McManus, J., Oppo, D.W., Francois, R., 2012. Strengthening of the Northeast Monsoon over the Flores Sea, Indonesia, at the time of Heinrich event 1. Geology 40 (7), 635–638.

Murton, J.B., Bateman, M.D., Dallimore, S.R., Teller, J.T., Yang, Z.R., 2010. Identification of Younger Dryas outburst flood path from Lake Agassiz to the Arctic Ocean. Nature 464 (7289), 740–743. http://dx.doi.org/10.1038/Nature08954.

Oppo, D.W., Schmidt, G.A., LeGrande, A.N., 2007. Seawater isotope constraints on tropical hydrology during the Holocene. Geophys. Res. Lett. 34 (13), L13701. http://dx.doi.org/10.1029/2007gl030017.

Oppo, D.W., Curry, W.B., 2012. Deep atlantic circulation during the Last Glacial maximum and deglaciation. Nature Education 3 (10), 1.

Otto-Bliesner, B.L., Brady, E.C., 2010. The sensitivity of the climate response to the magnitude and location of freshwater forcing: last glacial maximum experiments. Quat. Sci. Rev. 29 (1), 56–73.

Partin, J.W., Cobb, K.M., Adkins, J.F., Clark, B., Fernandez, D.P., 2007. Millennial-scale trends in west Pacific warm pool hydrology since the Last Glacial Maximum. Nature 449 (7161), 452–455. http://dx.doi.org/10.1038/Nature06164.

Rosenthal, Y., Boyle, E.A., Slowey, N., 1997. Temperature control on the incorporation of magnesium, strontium, fluorine, and cadmium into benthic foraminiferal shells from Little Bahama Bank: Prospects for thermocline paleoceanography. Geochim. Cosmochim. Acta 61 (17), 3633–3643.

Rosenthal, Y., Oppo, D.W., Linsley, B.K., 2003. The amplitude and phasing of climate change during the last deglaciation in the Sulu Sea, western equatorial Pacific. Geophys. Res. Lett. 30 (8), L1428. http://dx.doi.org/10.1029/2002gl016612.

Rosenthal, Y., Broccoli, A.J., 2004. Search of Paleo-ENSO. Science 304, 219–221.

Sarnthein, M., Grootes, P.M., Holbourn, A., Kuhnt, W., Kühn, Hartmut, 2011. Tropical warming in the Timor Sea led deglacial Antarctic warming and atmospheric CO_2 rise by more than 500 yr. Earth Planet. Sci. Lett. 302 (3), 337–348.

Schrag, D.P., Adkins, J.F., McIntyre, K., Alexander, J.L., Hodell, D.A., Charles, C.D., McManus, J.F., 2002. The oxygen isotopic composition of seawater during the Last Glacial Maximum. Quat. Sci. Rev. 21 (1–3), 331–342.

Shakun, J.D., Clark, P.U., He, F., Marcott, S.A., Mix, A.C., Liu, X., Otto-Bliesner, B., Schmittner, A., Bard, E., 2012. Global warming preceded by increasing carbon dioxide concentrations during the last deglaciation. Nature 484, 49–54. http://dx.doi.org/10.1038/nature10915.

Stager, J.C., Ryves, D.B., Chase, B.M., Pausata, F.S.R., 2011. Catastrophic drought in the Afro-Asian Monsoon Region during Heinrich Event 1. Science 331 (6022), 1299–1302. http://dx.doi.org/10.1126/Science.1198322.

Stanford, J.D., Rohling, E.J., Bacon, S., Roberts, A.P., Grousset, F.E., Bolshaw, M., 2011. A new concept for the paleoceanographic evolution of Heinrich event 1 in the North Atlantic. Quat. Sci. Rev. 30 (9–10), 1047–1066. http://dx.doi.org/10.1016/J.Quascirev.2011.02.003.

Steinke, S., Kienast, M., Groeneveld, J., Lin, L.C., Chen, M.T., Rendle-Buhring, R., 2008. Proxy dependence of the temporal pattern of deglacial warming in the tropical South China Sea: toward resolving seasonality. Quat. Sci. Rev. 27 (7–8), 688–700. http://dx.doi.org/10.1016/J.Quascirev.2007.12.003.

Stott, L., Poulsen, C., Lund, S., Thunell, R., 2002. Super ENSO and global climate oscillations at millennial time scales. Science 297, 222–226.

Stott, L., Cannariato, K., Thunell, R., Haug, G.H., Koutavas, A., Lund, S., 2004. Decline of surface temperature and salinity in the western tropical Pacific Ocean in the Holocene epoch. Nature 431 (7004), 56–59. http://dx.doi.org/10.1038/nature02903.

Stott, L., Timmermann, A., Thunell, R., 2007. Southern Hemisphere and deep-sea warming led deglacial atmospheric CO_2 rise and tropical warming. Science 318, 435–438. http://dx.doi.org/10.1126/science.1143791.

Tierney, J.E., Russell, J.M., Huang, Y., Damste, J.S.S., Hopmans, E.C., Cohen, A.S., 2008. Northern hemisphere controls on tropical southeast African climate during the past 60,000 years. Science 322 (5899), 252–255. http://dx.doi.org/10.1126/science.1160485.

Tierney, J.E., Oppo, D.W., LeGrande, A.N., Huang, Y., Linsley, B.K., 2012. The influence of Indian Ocean atmospheric circulation on Warm Pool hydroclimate during the Holocene epoch. J. Geophys. Res., Atmos. 177, D19108.

Visser, K., Thunell, R., Stott, L., 2003. Magnitude and timing of temperature change in the Indo-Pacific warm pool during deglaciation. Nature 421, 152–155.

Waelbroeck, C., Labeyrie, L., Michel, E., Duplessy, J.C., McManus, J.F., Lambeck, K., Balbon, E., Labracherie, M., 2002. Sea-level and deep water temperature changes derived from benthic foraminifera isotopic records. Quat. Sci. Rev. 21 (1–3), 295–305.

Wang, X., Edwards, R.L., Auler, A.S., Cheng, H., Ito, E., 2007. Millennial-scale interhemispheric asymmetry of low-latitude precipitation: speleothem evidence and possible high-latitude forcing. AGU, Washington, DC, pp. 279–295.

Wang, Y., Cheng, H., Edwards, R.L., He, Y., Kong, X., An, Z., Wu, J., Kelly, M.J., Dykoski, C.A., Li, X., 2005. The Holocene Asian Monsoon: links to Solar changes and North Atlantic climate. Science 308, 854.

Xu, J., Holbourn, A., Kuhnt, W.G., Jian, Z.M., Kawamura, H., 2008. Changes in the thermocline structure of the Indonesian outflow during Terminations I and II. Earth Planet. Sci. Lett. 273 (1–2), 152–162.

Xu, J., Kuhnt, W., Holbourn, A., Regenberg, M., Andersen, N., 2010. Indo-Pacific Warm Pool variability during the Holocene and Last Glacial Maximum. Paleoceanography 25, PA4230. http://dx.doi.org/10.1029/2010PA001934.

Yuan, D., Cheng, H., Edwards, R.L., Dykoski, C.A., Kelly, M.J., Zhang, M., Qing, J., Lin, Y., Wang, Y., Wu, J., Dorale, J.A., An, Z., Cai, Y., 2004. Timing, duration, and transitions of the Last Interglacial Asian Monsoon. Science 304, 575–578.

Zhang, R., Kang, S.M., Held, I.M., 2010. Sensitivity of climate change induced by the weakening of the Atlantic Meridional Overturning Circulation to cloud feedback. J. Climate 23, 378–389. http://dx.doi.org/10.1175/2009JCLI3118.1.